Dip-angle domain specularity filter design in relation with subsurface offset extended RTM

Raanan Dafni and William W. Symes, Rice University*

Summary

Common-image gathers (CIGs) in the dip-angle domain may be computed in relation with wave-equation migration methods such as RTM, extended by the subsurface offset. It involves the application of a post-migration local Radon transform on the subsurface offset extended image. In the dip-angle domain, seismic reflections are focused around the specular dip-angle of reflection. This focusing distinguishes them from any other event in the image space. We propose to incorporate the dip-angle information about the presence of specular reflections to eliminate noise and artifacts in the prestack image. We design a specularity filter in the dip-angle domain that recognizes and passes events associated with specular reflections, while supressing other sorts of non-specular signal. In particular, our filter provides a method for the suppression of kinematic artifacts, commonly generated by wave-equation migration in the subsurface offset domain.

Introduction

Prestack migration operators can be described as the adjoint of extended Born-type modeling operators, after extending the definition of the reflectivity to depend on more degrees of freedom (Symes, 2008; Stolk et al., 2009). One conventional and natural choice to extend the reflectivity is by the horizontal subsurface offset (Claerbout, 1985; Sava and Vasconcelos, 2011). It is defined as the horizontal offset vector connecting the sunken shot and receiver in the subsurface, and involves an action at a distance between the incident and scattered wavefields. A perfectly focused image is expected at the zero offset trace of the subsurface offset CIGs when the exact velocity model is used. A common difficulty that usually arises in computing subsurface offset CIGs is the appearance of kinematic artifacts away from the zero offset trace (Mulder, 2014). Like other coherent noise, these artifacts can impede velocity model optimization and their elimination might become a real challenge. Almomin and Biondi (2014) addressed this problem in the context of tomographic full waveform inversion (TFWI). They derived a preconditioner for the acoustic wave-equation that compensates for biased amplitude behavior of the reflection coefficient. Their preconditioned inversion algorithm improved significantly the TFWI convergence rate by suppressing the kinematic artifacts.

In this study, we propose a different approach for this matter. It is suggested to distinguish the specular reflections in the dip-angle domain by their well-defined specular dip direction, while rejecting any other sort of non-specular signal in the image (like the mentioned kinematic artifacts). Incorporating dip-angle information for image quality enhancement was already introduced in the past by several authors (Qin et al., 2005; Bienati et al, 2009; Koren and Ravve, 2011; Dafni and Reshef, 2014). However, they are all associated with Kirchhoff migration methods. They rely on the stationary phase assumption implying that the Kirchhoff integral over the dip-angles is constructive only along a limited dip aperture around the specular angle.

Dip-angle decomposition is not restricted to Kirchhoff migration only. Dafni and Symes (2016) proposed to decompose dip-angle CIGs in relation with extended wave-equation migration in the subsurface offset domain. Forward and inverse Radon transform operators were formulated to transform the subsurface offset extended image to the dip-domain and back. We follow their proposal and demonstrate the relationship between wave-equation migration methods and the dip-angle domain. A specularity filter is designed in the dip-domain to suppress noise and non-specular contributions to the image. In particular, the filter's application is directed to effectively eliminate the kinematic artifacts. We also exemplify the robustness of the filter when velocity errors are present. The filter rejects the kinematic artifacts without impairing the reflection's defocusing/moveout information.

The Formation of Kinematic Artifacts

The focusing of the seismic events in the subsurface offset domain, due to a perfectly known velocity model, is often observed as incomplete when some signal "leaks" to non-zero offsets. It is demonstrated via a tow-layers synthetic example, consisting of a -5º dipping reflection interface. The synthetic data in this example were simulated by an acoustic Born modeling operator. For imaging, we used a subsurface offset extended RTM operator and the true velocity model. Figure 1a presents on the left side the resulting image section along with a single subsurface offset CIG, calculated at the 4km mark. The reflector's image is well positioned in space and focused at zero offset. However, a weak but considerable signal is clearly "leaking" and contaminating the non-zero offsets (marked by the red arrows). We consider this leakage as kinematic artifacts that emerge due the truncation of the seismic data at the acquisition geometry by a maximum offset (Mulder, 2014). The artifacts are coherent and give a false image of the reflector. They have an elliptic shape under the assumption of homogeneous medium. Transformation to the scattering-angle domain is achieved by a Radon

transform operator that decompose the angles out of the subsurface offset CIGs (Sava and Fomel, 2003; Dafni and Symes, 2016). We follow this transformation to decompose the scattering-angle CIGs in our example. The angle gather, computed at the 4km mark, is shown on the right side of Figure 1a. A flat event is shown in the angle-domain, indicating the assurance of the migration velocity. The kinematic artifacts were transformed into hyperbolic curves (marked by the red arrows) that peak at the maximum angle of illumination.

We repeat the migration by using a 10% too-high and 10% too-low velocity models. The imaging results are shown in Figures 1b and 1c, respectively. The image sections are displayed to the left of the subsurface offset CIGs and the scattering-angle CIGs. The erroneous migration velocity impairs the focusing/flatness of the image in the subsurface offset or the scattering-angle domain, respectively. Nevertheless, the kinematic artifacts are as prominent when velocity errors are present. They still show an elliptic/hyperbolic behavior. Their considerable presence might decelerate any attempt of velocity model optimization.

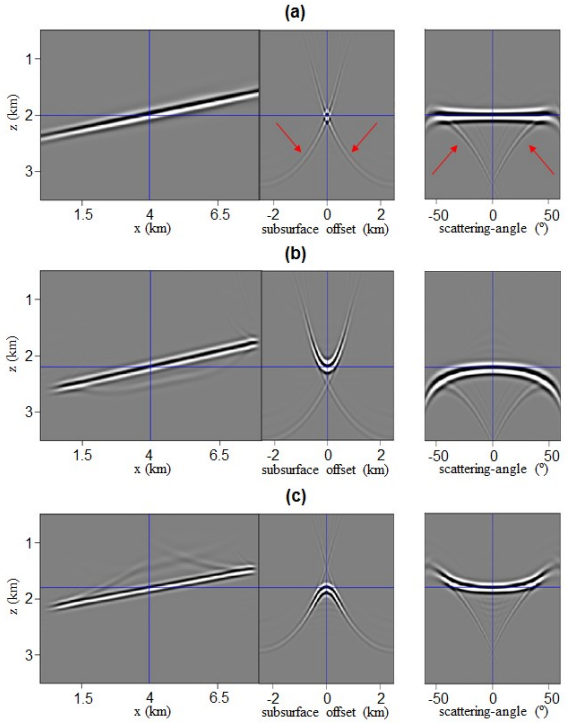

Figure 1: Imaging of a -5º dipping reflector by (a) true (b) 10% too-high and (c) 10% too-low migration velocity. The subsurface offset image is presented to the left of the scattering-angle image.

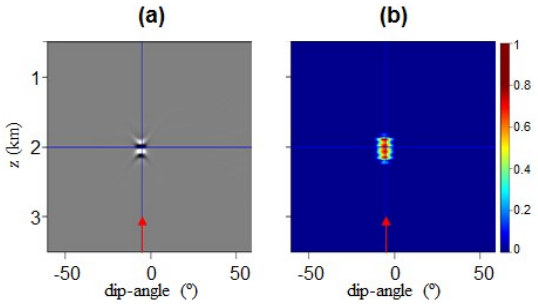

Figure 2: Imaging of a -5º dipping reflector by the true velocity. (a) Dip-angle CIG, calculated at the 4km mark. (b) The corresponding Semblance profile, employed as the specularity filter.

Specularity Filter Design

Wave-equation migration methods, such as RTM, do not result in noise-free images. The kinematic artifacts are just one example supporting this claim. We propose to recognize and suppress artificial events in the image by a specular criterion imposed in the dip-angle domain. We follow Dafni and Symes (2016) dip-angle decomposition technique to transform the subsurface offset extended image to the dip-angle domain. It implies about a relation between wave-equation imaging methods and the dip-angle domain. The transformation is demonstrated in Figure 2a. The dip-angle CIG in the figure is decomposed at the 4km mark from the subsurface offset extended image shown in Figure 1a. Seismic reflections respond in the dip-angle domain as spot-like events that indicate the specular dip direction of the reflection (Dafni and Symes, 2016). Since a -5º dipping reflector is embedded in our example, a clear spot is recognized in the figure at the -5º dip-angle trace (marked by the red arrow). A well-defined specular dip profile is extracted by measuring the strength of the dip focusing via the Semblance coefficient S, as a function of depth and dip-angle ν within each dip-angle CIG:

$$S(z,\nu)=\frac{1}{N_\nu}\frac{\sum_{iz=z-N_z}^{z+N_z}\left(\sum_{i\nu=\nu-N_\nu}^{\nu+N_\nu}CIG(iz,i\nu)\right)^2}{\sum_{iz=z-N_z}^{z+N_z}\sum_{i\nu=\nu-N_\nu}^{\nu+N_\nu}CIG^2(iz,i\nu)}. \qquad (1)$$

This local Semblance formula depends on the choice of depth half-window size N_z and dip half-window size N_ν. The formula is designed to detect events that have less than a cycle of oscillation as a function of dip, over the calculation window. The spot-like events in the dip-domain oscillate entirely in the vertical direction, regardless of how steep the reflector is dipping. It is dictated by the stationary phase of reflections at the specular dip. Figure 2a demonstrates that behavior by showing an event with more than a full oscillation, but it is entirely vertical. Therefore, the event is locally coherent in dip. The extent of the

heuristic calculation window is predefined by the user, usually in accordance with the resolution of the events in the dip-domain (i.e., the spots size). In the examples presented here we used N_z=25m and N_v=6º. Figure 2b presents the Semblance profile calculated with respect to the dip-angle CIG in Figure 2a, and according to equation 1. The Semblance profile highly correlates with the dip-angle image and peaks at the specular angle of -5º. Therefore, we propose to employ the Semblance as a dip-domain specularity filter, applied on the dip-angle CIG as a weighting function. This filter is expected to enhance strong specular events while suppressing the weak ones.

Specularity Filter Application

The workflow involving the application of the specularity filter includes a forward and inverse transformation to the dip-angle domain. First, the subsurface offset CIGs are transformed to the dip-domain, where the filter is constructed and applied. Then, the filtered dip-angle CIGs are inverse transformed back to the subsurface offset domain for further noise-free analysis. The application of the filter is exemplified first in relation with the dipping reflector example. The image is filtered in the dip-domain by the specularity filter (see Figure 2), and transformed back to the subsurface offset domain. The results are shown on the left side of Figure 3a. There is no evidence whatsoever to the contamination of the kinematic artifacts. The noise-free image is perfectly focused at zero subsurface offset. We further transform the filtered image to the scattering-angle domain, as shown on the right side of the figure. The scattering-angle image yields only the expected flat event at the true depth of reflection. No remnant imprint is left to indicate about the artificial hyperbolic curves that were recognized originally.

The specularity filter success to distinguish the specular reflections when wrong migration velocity is used is tested next. We follow the same filtering workflow suggested above, and use as input the subsurface offset extended images associated with the wrong migration velocities (shown on the left in Figures 1b and 1c). The filtered image associated with the too-fast and too-slow velocity is presented in Figures 3b and 3c, respectively. The subsurface offset extended images are presented to the left of the scattering-angle images. Although the reflector was wrongly migrated due to the erroneous velocity, the specularity filtering is still shown as effective and robust. The non-specular artifacts were removed without harming the essential defocusing/moveout information about the velocity error. We expect these artifact-free gathers to alleviate some of the difficulties involving the convergence of velocity model optimization methods in relation with subsurface offset extended imaging.

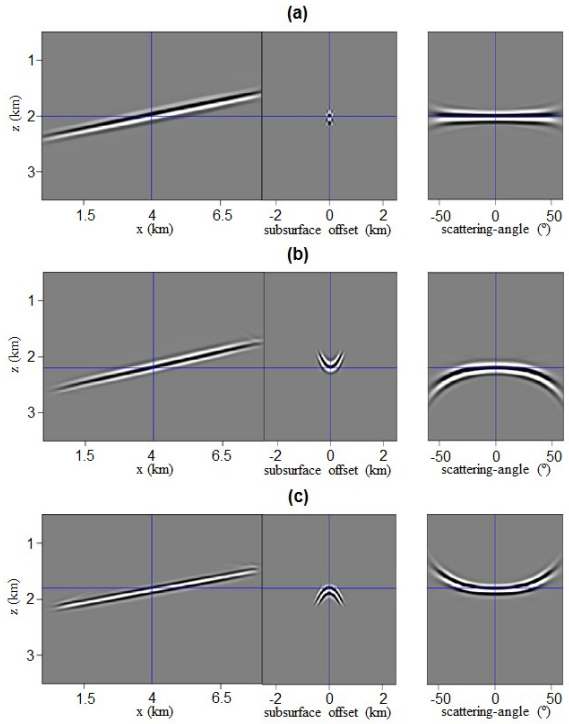

Figure 3: Specularity filtering in relation with (a) true (b) 10% too-high and (c) 10% too-low migration velocity. The filtered subsurface offset image to the left of the scattering-angle image.

In the next example we test the specularity filter competence to handle random and coherent noise inserted artificially to the image. Our synthetic model includes four curved reflectors and a perfectly known velocity model. We calculated and migrated the data using the same modeling and migration operators as in the previous example. Noise was added to the resulting subsurface offset extended image, as shown in Figure 4. At the top part of the figure the noisy image section is provided above a set of three subsurface offset CIGs, calculated at the locations marked with dashed lines. At the bottom of Figure 4 we also present the transformed set of noisy scattering-angle CIGs. The four reflection events are identified behind the evident noise in the image. The random noise was set to peak around the zero offset trace, where the true reflection events focus. The coherent noise was inserted as a fake reflection event, focused coherently at a non-zero subsurface offset of -500m (marked by the red arrows). This fake event was transformed to the angle-domain as an inclined event, rather than flat. In real life, this might enforce additional (but obviously not required) velocity optimization steps, by considering this event as true. In Figure 5 we present the corresponding set of dip-angle CIGs, and the construction of the specularity filter. Four specular spots are clearly recognized. They indicate the

local dip direction of the subsurface reflectors. The noise is still present in the dip-domain but without a clear dip direction. Therefore it is expected to be filtered. We applied the specularity filter and inverse transformed the image back to the subsurface offset domain. Figure 6 shows the filtered image and the transformation to the scattering-angle domain. The random noise was significantly suppressed, and no evidence remains for the fake event. Furthermore, the kinematic artifacts were removed as well. Comparing Figures 4 and 6 emphasizes the comprehensive job done by the specularity filter.

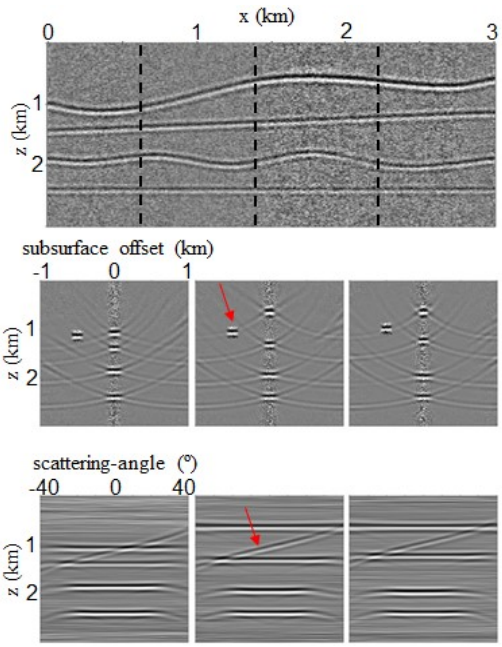

Figure 4: Random and coherent noise contaminates the subsurface offset extended image (top and middle parts). The noise is as prominent in the scattering-angle domain as well (bottom).

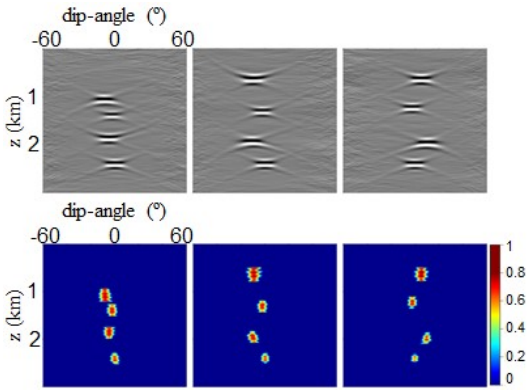

Figure 5: The noisy set of dip-angle CIGs above the coresponding secularity filter.

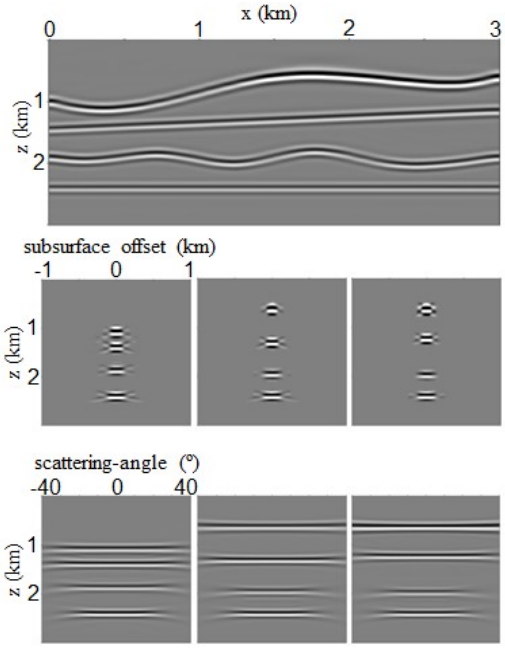

Figure 6: The specularity filtered subsurface offset extended image (top and middle parts). The noise was succssefully eliminated in the scattering-angle domain as well (bottom).

Conclusions

Post-migration analysis of CIGs in the dip-angle domain is not restricted solely to Kirchhoff migration. It can also be based on wave-equation migration methods (like RTM), extended by the subsurface offset. Dip-angle information, extracted from dip-angle CIGs, is directly related to the subsurface structure and distinguishes specular reflections from coherent or incoherent noise. Incorporating this information into the conventional migration velocity and amplitude analysis is essential for their success. Our methodology characterizes specular reflections as spot-like events in the dip-angle domain, indicating the local dip in the subsurface. A specularity filter was designed in the dip-domain to pass only energy related to specular reflection events. The filter was applied to suppress kinematic artifacts, which commonly emerge in subsurface offset extended imaging, regardless of the migration velocity assurance. We also demonstrated the robustness of the filter to enhance the image quality by eliminating random and coherent noise in the image space.

Acknowledgments

We are grateful to the sponsors of The Rice Inversion Project (TRIP) and Shell International Exploration and Production Inc. We also thank the Israeli Ministry of National Resources for partial financial support.